



Article

Genome-Scale CRISPR Knockout Screening Identifies BACH1 as a Key Regulator of Aflatoxin B₁-Induced Oxidative Damage

Jinfu Zhang^{1,2,†}, Siyi Hu^{3,†}, Changzhi Zhao¹, Yuan Zhou¹, Lu Zhang¹, Hailong Liu¹, Peng Zhou¹, Sheng Li¹, Liangliang Fu¹, Zhuqing Zheng¹, Yue Xiang¹, Xuwen Xu^{1,2}, Jinxue Ruan¹, Xinyun Li^{1,4,5}, Lvhui Sun⁴, Gang Cao⁴, Shuhong Zhao^{1,2,4,5,*}, Xu Wang^{3,*} and Shengsong Xie^{1,2,4,5,*}

¹ Key Laboratory of Agricultural Animal Genetics, Breeding and Reproduction of Ministry of Education & Key Lab of Swine Genetics and Breeding of Ministry of Agriculture and Rural Affairs, Huazhong Agricultural University, Wuhan 430070, China

² Guangdong Laboratory of Lingnan Modern Agriculture, Guangzhou 510642, China

³ National Reference Laboratory of Veterinary Drug Residues (HZAU) and MAO Key Laboratory for Detection of Veterinary Drug Residues, Huazhong Agricultural University, Wuhan 430070, China

⁴ Hubei Hongshan Laboratory, Huazhong Agricultural University, Wuhan 430070, China

⁵ The Cooperative Innovation Center for Sustainable Pig Production, Huazhong Agricultural University, Wuhan 430070, China

* Correspondence: shzhao@mail.hzau.edu.cn (S.Z.); wangxu@mail.hzau.edu.cn (X.W.); sxxie@mail.hzau.edu.cn (S.X.)

† These authors contributed equally to this work.

Abstract: Aflatoxin B₁ (AFB₁) is amongst the mycotoxins commonly affecting human and animal health, raising global food safety and control concerns. The mechanisms underlying AFB₁ toxicity are poorly understood. Moreover, antidotes against AFB₁ are lacking. Genome-wide CRISPR/Cas9 knockout screening in porcine kidney cells identified the transcription factor BTB and CNC homolog 1 (BACH1) as a gene required for AFB₁ toxicity. The inhibition of BACH1 expression in porcine kidney cells and human hepatoma cells resulted in increased resistance to AFB₁. BACH1 depletion attenuates AFB₁-induced oxidative damage via the upregulation of antioxidant genes. Subsequently, virtual structural screening identified the small molecule 1-Piperazineethanol, α -[(1,3-benzodioxol-5-yl)oxy)methyl]-4-(2-methoxyphenyl) (M2) as an inhibitor of BACH1. M2 and its analogues inhibited AFB₁-induced porcine and human cell death in vitro, while M2 administration significantly improved AFB₁-induced symptoms of weight loss and liver injury in vivo. These findings demonstrate that BACH1 plays a central role in AFB₁-induced oxidative damage by regulating antioxidant gene expression. We also present a potent candidate small-molecule inhibitor in developing novel treatments for AFB₁ toxicity.

Keywords: AFB₁; BACH1; CRISPR screening; inhibitor



Citation: Zhang, J.; Hu, S.; Zhao, C.; Zhou, Y.; Zhang, L.; Liu, H.; Zhou, P.; Li, S.; Fu, L.; Zheng, Z.; et al. Genome-Scale CRISPR Knockout Screening Identifies BACH1 as a Key Regulator of Aflatoxin B₁-Induced Oxidative Damage. *Antioxidants* **2022**, *11*, 1787. <https://doi.org/10.3390/antiox11091787>

Academic Editor: Stanley Omaye

Received: 14 August 2022

Accepted: 7 September 2022

Published: 10 September 2022

Publisher's Note: MDPI stays neutral with regard to jurisdictional claims in published maps and institutional affiliations.



Copyright: © 2022 by the authors. Licensee MDPI, Basel, Switzerland. This article is an open access article distributed under the terms and conditions of the Creative Commons Attribution (CC BY) license (<https://creativecommons.org/licenses/by/4.0/>).

1. Introduction

Aflatoxins are secondary metabolites produced mainly by the fungi *Aspergillus flavus* and *Aspergillus parasiticus*, four of which are known to occur naturally, including aflatoxin B₁ (AFB₁), B₂ (AFB₂), G₁ (AFG₁), and G₂ (AFG₂) [1,2]. AFB₁ exhibits the highest toxicity and is an unavoidable contaminant in foods and livestock feeds, endangering human and animal health [3]. For instance, AFB₁ is highly carcinogenic and can contribute to the development of hepatocellular carcinoma (HCC) [4]. The toxic effects of AFB₁ are both dose- and time-dependent, and aflatoxicosis can be either acute or chronic. Exposure to AFB₁ affects multiple organs like kidneys, liver, heart, testes, and ovaries, causing mutagenesis, growth retardation, and reproductive damage [5,6]. Moreover, AFB₁ toxicity significantly suppresses the immune system, increasing the risk of acquiring concurrent infectious diseases [7].

In addition to the AFB₁-associated effects in humans, severe health issues such as hepatotoxicity, teratogenicity, and immunotoxicity occur in animals [6,8,9]. Pigs exposed to aflatoxin-contaminated feed are highly susceptible to secondary infections [10]. AFB₁ can also negatively impact meat quality due to associated oxidative stress, inflammation, and the dysregulation of gut microbiota and dysbiosis in animals [11,12]. Various physical, chemical, and biological approaches to preventing AFB₁ contamination have been developed [13–15]. For instance, transgenic pigs expressing aflatoxin-detoxifying enzyme (ADTZ) exhibit resistance to AFB₁ toxicity [16]. Nevertheless, economic losses and threats to public health caused by AFB₁ contamination persist [13,17]. Thus, further efforts to identify the molecular mechanisms underlying AFB₁ toxicity are necessary for reducing aflatoxicosis and decreasing the risk to animal and human health.

AFB₁ requires metabolic activation (biotransformation) by cytochrome P450 enzymes to generate AFB₁-exo-8,9-epoxide (AFBO), which forms adducts through binding with DNA, RNA, and proteins [18]. The detoxification of AFBO mainly occurs through conjugation with glutathione (GSH) mediated by glutathione S-transferase (GST), a phase II conjugative (detoxification) enzyme [19]. In addition, except for AFBO, animals can metabolize aflatoxin into relatively less toxic intermediates or metabolites, such as aflatoxin M₁ (AFM₁) [20]. Previous studies have revealed that AFB₁ can induce the overexpression of *CYP1A1* and *CYP1A2* genes, accompanied by the increased transcription of Aryl hydrocarbon receptor (AhR), which was linked to AFB₁-related toxicity in a recent genome-wide loss-of-function screening [21,22]. Another study identified cyclooxygenase-2 (COX-2) as a factor in AFB₁-induced mitophagy and lipid accumulation [21,22]. It has also been shown that caveolin-1 plays an essential role in the AFB₁-induced apoptosis of hepatic cells via the regulation of oxidation and autophagy [23]. Nonetheless, the mechanisms involved in AFB₁ toxicity remain poorly understood.

In this study, we adopted a high-throughput forward screening strategy to identify the host factors required for AFB₁-induced cell death using our previously designed porcine genome-scale CRISPR/Cas9 knockout (PigGeCKO) library [24]. We found that the transcription factor BACH1 was paramount in AFB₁ cytotoxicity. Knockout (KO) of *BACH1* could inhibit AFB₁-induced oxidative damage through the transcriptional upregulation of antioxidant genes. Moreover, structure-based virtual screening led to the identification of several potential small-molecule inhibitors of BACH1 and confirmed the effectiveness of 1-Piperazineethanol, α -[(1,3-benzodioxol-5-yloxy)methyl]-4-(2-methoxyphenyl) (hereinafter called M2) as an inhibitor both in vitro and in vivo. Accordingly, BACH1 is a potential drug target for AFB₁-induced oxidative damage. Moreover, M2 can serve as an efficient inhibitor of AFB₁.

2. Materials and Methods

2.1. Plasmid Construction

Lentivirus small-guide RNA (sgRNA) expression vectors were generated by digesting the lenti-sgRNA-EGFP and LentiCRISPRv2 plasmids (Addgene #52961) using the *BbsI* and *BsmBI* restriction enzymes, respectively. The paired sgRNA oligonucleotides were annealed and cloned into the linearized vector. These sgRNAs were designed by sgRNACas9-AI (<http://123.57.239.141:8080/home>, accessed on 6 December 2019). The sgRNA sequences are listed in Table S1.

2.2. Cell Culture and Transfection

The porcine Kidney-15 (PK-15), human embryonic kidney 293T (HEK293T), and Huh7 cell lines were purchased from the Cell Bank of the Chinese Academy of Sciences (Shanghai, China). These cell lines were tested for mycoplasma and maintained at 37 °C with 5% CO₂ in Dulbecco's Modified Eagle Medium (DMEM) (Cat No: C11995500BT, Gibco, Beijing, China) supplemented with 10% fetal bovine serum (FBS) (Cat No: 10270-106, Gibco), 100 U/mL penicillin and 100 µg/mL streptomycin (Cat No: 15140122). The

JetPrime reagent (Cat No: B180306, PolyPlus) was used for transfection according to the manufacturers protocol.

2.3. Genome-Wide CRISPR/Cas9 Screening

Genome-wide CRISPR/Cas9-based screening in PK-15 cells was conducted using the PigGeCKO lentiviral sgRNA library as previously described [24]. The PigGeCKO library contains 85,674 single-guide RNAs targeting 17,743 protein-coding genes, 11,053 long ncRNAs, and 551 miRNAs. A total of $\sim 2 \times 10^8$ PK-15 cells stably expressing Cas9 (hereafter referred to as PK-15-Cas9) were seeded into T225 flasks and infected with the sgRNA lentiviral library at a multiplicity of infection (MOI) of 0.3. Three days post-infection, GFP-positive cells were collected by fluorescence-activated cell sorting (FACS), reseeded into 100 mm dishes, and preserved and the coverage was examined of the mutant cell libraries. For the CRISPR screening, a total of $\sim 1 \times 10^8$ mutant cells were exposed to AFB₁ (Cat No: 1162-65-8) at 0.2 $\mu\text{g}/\text{mL}$, and the toxin was refreshed daily until all the PK-15-Cas9 (Control) died. The surviving mutant cells were then exposed to two additional rounds of AFB₁ at different concentrations (Round 2 at 1 $\mu\text{g}/\text{mL}$ and round 3 at 6 $\mu\text{g}/\text{mL}$). Genomic DNA was isolated from $\sim 1 \times 10^6$ surviving cells from each round of exposure, integrated sgRNA sequences obtained by polymerase chain reaction (PCR) and decoded by Illumina-based sequencing. The remaining surviving mutant cells were cultured in medium containing 15 $\mu\text{g}/\text{mL}$ H₂O₂ until all the control cells died. The surviving cells were collected for genomic DNA isolation and the identification of sgRNAs by Illumina-based sequencing.

2.4. Generation of PK-15 and Huh7 KO Cell Lines by CRISPR/Cas9 Technology

The sgRNA sequence targeting the porcine *BACH1* was cloned into the linearized lenti-sgRNA-EGFP vector, and lentivirus was assembled to infect PK-15-Cas9 cells. GFP-expressing cells were enriched by FACS on the 3rd day post-infection and seeded in 96-well plates to generate clonal KO cells. Approximately 7 days after infection, the genotypes of the cell colonies were analyzed by extracting genomic DNA using the TIANamp Genomic DNA Kit (Cat No: DP304, TIANGEN, Beijing, China), and the nucleotide sequences were revealed by Sanger sequencing (Tsingke, Wuhan, China). Mutant colonies identified from the sequences were characterized by homozygous TA clone sequencing. The sgRNA sequence targeting porcine *BACH1* was also cloned into the linearized lentiCRISPRv2 and generated the PK-15 mutant colonies without a green fluorescent protein (GFP) label. The sgRNA targeting the human *BACH1* gene was cloned into the linearized lentiCRISPRv2, and lentivirus was assembled to infect the Huh7 cells. On the 3rd day post-infection, infected cells were selected using 2.5 $\mu\text{g}/\text{mL}$ puromycin to generate the human *BACH1* KO pooled cells. The Sanger sequencing primers used are shown in Table S1.

2.5. Cell Counting Kit-8 (CCK-8) Viability Assay

Approximately 1×10^4 cells/well were seeded in 96-well flat-bottomed plates (Cat No: 701001, NEST, Wuxi, China) and incubated at 37 °C + 5% CO₂ for 24 hours (h) to obtain 50–60% confluence. The AFB₁ and other inhibitors were added to all the test sample cells except the control group and incubated for 36 h. The CCK-8 stock solution (Cat No: KGA317, KeyGEN, Jiangsu, China) was diluted 1:10 in unsupplemented DMEM to make the CCK-8 working solution. 100 μL of the CCK-8 working solution was added to each well, and the plate was incubated for 1 h at 37 °C. Absorbance at 450 nm was measured using a microplate reader (EnVision, PerkinElmer, Waltham, MA, USA). Absolute (100%) viability was defined as the absorbance of the control groups.

2.6. Flow Cytometry Analysis for Reactive Oxygen Species

Approximately 1×10^5 cells/well were seeded in 12-well plates for 24 h to obtain 50–60% confluence. The wells were treated with 0.1 $\mu\text{g}/\text{mL}$ AFB₁, and the plates were incubated at 37 °C for 36 h. The cell monolayer was detached using 0.25% trypsin without EDTA (Cat No: 15050-065, Gibco) and resuspended in supplemented DMEM. Reactive oxygen

species (ROS) were detected by adding the ROS detection green fluorescent probe reagent (Cat No: KGAF018, KeyGEN) and incubating in a water bath at 37 °C for 30 minutes (min), with gentle agitation at 3 min intervals, away from light. The excess probe was discarded by washing the cells 5-times at $650 \times g$ for 10 min in pre-chilled phosphate-buffered saline (PBS). The cell pellet was resuspended in FACS buffer to make a homogenous suspension analyzed in a BD Accuri C6 Plus flow cytometer (Becton, Dickinson and Company, Franklin Lakes, NJ, USA) using the Fluorescein (FITC) green fluorescence channel. FCS files were analyzed in FlowJoV10 analysis software.

2.7. Structure-Based Virtual Screening

To identify inhibitors that confer high resistance to AFB₁ exposure, structure-based virtual screening was conducted targeting BACH1 using the known structure of human BACH1 protein obtained from the RCSB protein database (PDB) (<https://www.rcsb.org/>, accessed on 30 May 2020). The Specs small-molecule compound database of 55,024 compounds was used as the ligand library for virtual docking with human BACH1 (<https://specs.net/>, accessed on 30 May 2020). The virtual screening was performed using the Surflex-Dock of SYBYL-X 2.0 (Tripos, St. Louis, MO, USA) based on the crystal structure of human BACH1 (PDB ID: 2IHC). The SYBYL software was used to assign the standard AMBER atomic partial charges on the human BACH1 protein and the Gasteiger–Hückel atomic partial charges on the ligand candidates to be docked. After the preparation, the docking was performed using the default settings, and the figures were generated using PyMol software (<https://pymol.org/2/>, accessed on 30 May 2020). The abbreviations and synonyms of corresponding inhibitors (M1, M2, M3, M4, M5, M6, M7, M8, and M9) are shown in Table S2.

2.8. RNA Sequencing and Transcriptome Analysis

PK-15 and BACH1-KO cells were seeded into 6-well plates (Cat No: 703001, NEST, Wuxi, China) in triplicate to 60% confluence and treated with 2 µg/mL AFB₁. The cells were harvested 36 h post-treatment, and total RNA was isolated using TRIzol RNA Isolation Reagent (Cat No: 15596-026, Invitrogen). Library construction and sequencing were conducted at the National Key Laboratory of Crop Genetic Improvement using the MGISEQ-2000RS platform. Sequence quality was assessed using FastQC (v0.11.7, <https://sourceforge.net/projects/fastqc.mirror/>, accessed on 1 September 2020), and quality trimming was performed using the FASTX-Toolkit (v0.0.14, http://hannonlab.cshl.edu/fastx_toolkit/, accessed on 1 September 2020) to remove bases with a Phred33 score of less than 30 while retaining the resulting reads of at least 50 bases in length. The quality-trimmed reads were mapped against the reference genome of *Sus scrofa* (v11.1) using HISAT2 (v2.1.0, <http://daehwankimlab.github.io/hisat2/>, accessed on 15 September 2020). Gene expression profiling was based on the number of reads. Fragments per kb of exon model per million mapped reads (FPKM) was used to estimate the expressed values and transcript levels using SAMtools (v1.7, <https://www.htslib.org/>, accessed on 15 September 2020) and HTSeq-count (v0.9.1, <https://github.com/htseq/htseq>, accessed on 15 September 2020). Differently expressed genes (DEGs) were obtained using DESeq2 (v1.30.1, <https://bioconductor.org/packages/release/bioc/html/DESeq2.html>, accessed on 20 September 2020) with a *p* value cutoff ≤ 0.05 and an absolute fold change of ≥ 1 . The STRING database (<https://string-db.org>, accessed on 25 September 2020) was used to construct the DEGs' protein–protein interaction (PPI) networks, and the core genes from gene set enrichment analysis (GSEA) (<https://www.gsea-msigdb.org/gsea>, accessed on 25 September 2020); then, the degree values were determined using Cytoscape v3.7.2 (https://cytoscape.org/what_is_cytoscape.html, accessed on 25 September 2020).

2.9. Quantitative Real-Time PCR Assay

Total cell RNA was extracted using TRIzol Reagent (Cat No: 15596-026, Invitrogen, Waltham, MA, USA). The cDNAs were synthesized using the PrimeScript™ RT reagent Kit

with gDNA Eraser (Cat No: RR047A, TaKaRa, Kusatsu, Japan) in a total reaction volume of 20 μ L. Each RT-qPCR reaction was carried out with 50 ng of cDNA and 5 nM primer pairs using SYBR Green Mix (Cat No: Q711-02-AA, Vazyme, Nanjing, China). The results were monitored using a CFX384 Real-Time PCR Detection System (Bio-Rad, Hercules, CA, USA) programmed for 1 cycle of 10 min at 95 °C, followed by 39 cycles of 10 s at 95 °C and 10 s at 60 °C. The relative expression levels were calculated using the $2^{-\Delta\Delta C_t}$ method. The *Glyceraldehyde-3-phosphate dehydrogenase (GAPDH)* gene was used as a normalization control. All primers used in quantitative PCR are listed in Table S1.

2.10. Western Blot Analysis

After treatment, cells were collected, and the total proteins were extracted using RIPA solution (Servicebio, Wuhan, China) containing a mixture of protease phosphatase inhibitors (Beyotime, Nanjing, China). A BCA protein assay kit was used to measure the total concentrations of proteins according to the manufacturer's instructions. Twenty micrograms of cellular protein from each group was electro-blotted onto a PVDF membrane (Millipore, Burlington, MA, USA) following separation on 10% SDS-PAGE (Sangon Biotech, Shanghai, China). The membranes were blocked with 5% BSA in 0.1% Tween 20/Tris-buffered saline (TBST) for 2 h at room temperature and then incubated with either anti-BACH1 ((F-9): sc-271211) or anti-HOMX1 (10701-1-AP) antibodies overnight at 4 °C. Afterwards, samples were washed thrice with 0.1% TBST and incubated with secondary antibodies (1:2000) (Beyotime, Nanjing, China) at room temperature for 2 h. The enhanced chemiluminescence kit (Cat No: WBKLS0500) was used to visualize the protein bands.

2.11. Edu Cell Proliferation Assay

To assess cell proliferation, BACH1-KO and PK-15 cells were seeded into 12-well plates. The cells were maintained in DMEM with 10% FBS, 100 U/mL penicillin and 100 μ g/mL streptomycin, incubated at 37 °C with 5% CO₂. After 24 h, EdU cell proliferation assays were performed using the BeyoClick™ EdU Cell Proliferation Kit with Alexa Fluor 555 (Cat No: C0075S, Beyotime) according to the manufacturer's protocol. The cell nuclei were stained with 4',6-diamidino-2-phenylindole (DAPI) (Cat No: C1005, Beyotime) for 10 min at room temperature in the dark. Stained cells were visualized under a fluorescence microscope (DP80, Olympus, Tokyo, Japan). The proportion of EdU-positive cells were calculated in ImageJ software (three independent wells were imaged, and one random field per well was captured for each experimental phase).

2.12. Immunofluorescence Assay

Differences in AFB₁-DNA adducts in BACH1-KO and WT cells were assessed with immunofluorescence. Cells were seeded in a 24-well cell culture plate with pre-attached cell slides. The plated cells were treated with 1 μ g/mL AFB₁ diluted with 2% FBS in DMEM and incubated for 36 h at 37 °C + 5% CO₂. The cells were then fixed in 4% paraformaldehyde at 4 °C for 10 min and permeabilized at 4 °C for 10 min in cold 0.3% Triton X-100. This was followed by incubating with anti-AFB₁ antibody (Cat No: NB600-443, NOVUS, Saint Louis, MO, USA, 1:200) at 4 °C overnight. The primary antibodies were detected using Cy3 conjugated Goat anti-Mouse IgG (Cat No: HA1102, HUABIO, Hangzhou, China, 1:1000). Cell nuclei were counter-stained with DAPI (Cat No: G1012, Servicebio) for 10 min at room temperature in the dark. The slides were mounted with an anti-fluorescence quenching mountant and observed under a fluorescence microscope (Olympus, Tokyo, Japan) using the 40 \times objective lens. The proportion of fluorescing cells was calculated using ImageJ software on three independent slides, each with two or three random fields of view for each experimental group.

2.13. M2 Anti-AFB₁ In Vivo Experiment

Sprague-Dawley (SD) rats were used for in vivo experiments. The rats were stratified into five groups, namely, control, dimethyl sulfoxide (DMSO), M2, AFB₁, and AFB₁ + M2.

There were five rats in each group. The rats were acclimatized to the laboratory environment for 3 days with routine clinical scoring. Each group was inoculated with the appropriate material, i.e., saline, DMSO, M2 (20 mg/kg.bw intraperitoneal injection), AFB₁ (5 mg/kg.bw by gavage), or the combination of AFB₁ and M2, respectively. Gross sections of rat liver were collected, stained with hematoxylin and eosin (H&E), and assessed for pathological changes. Additionally, immunohistochemistry to detect AFB₁-DNA adduct and the extraction of liver tissue proteins for malondialdehyde (MDA) detection were conducted.

2.14. Hematoxylin and Eosin (H&E) Staining and Immunohistochemistry

The SD rats were euthanized and their liver tissue collected, fixed in 4% paraformaldehyde, and embedded in paraffin wax. Subsequently, the liver tissue was stained with H&E to make pathological sections. Sections were observed and captured using the Olympus BX53 microscope. Immunohistochemistry was performed on paraffin-embedded sections using an indirect immunoperoxidase method. The same embedded liver tissues were stained with anti-AFB₁ antibody (Cat No: NB600-443, NOVUS, Saint Louis, MO, USA, 1:200) to detect changes of AFB₁-DNA adducts.

2.15. Statistical Analysis

Statistical analysis was performed using R programming language. The means \pm S.D. were determined for each treatment group. Two-tailed Student's *t*-test was used to determine significant differences between treatment and control groups (* $p < 0.05$; ** $p < 0.01$; *** $p < 0.001$; **** $p < 0.0001$; ns, no significant).

3. Results

3.1. Genome-Scale CRISPR Screening Identifies Targets Required for AFB₁-Induced Cell Death

To systematically identify the host genes required for AFB₁-induced cell death, we performed genome-wide CRISPR KO screening in the porcine kidney (PK)-15 cells stably expressing Cas9 (hereafter referred to as PK-15-Cas9), as described in previous work [24] (Figure 1A). The overall CRISPR screening strategy is illustrated in Figure 1A. We first performed three rounds of challenge with AFB₁, using untreated PK-15-Cas9 cells as a negative control to confirm that cell death was attributable to AFB₁ exposure in each round of treatment. A total of 3 rounds of the AFB₁ challenge were carried out with increasing doses of 0.2 $\mu\text{g/mL}$, 1 $\mu\text{g/mL}$, and 6 $\mu\text{g/mL}$, respectively (Figure 1A). Since oxidative damage caused by AFB₁ is a central mechanism of AFB₁-induced cell death [25], we sought to identify the genes involved in AFB₁-induced oxidative damage. Thus, the surviving cells in the second round were simultaneously exposed to hydrogen peroxide (H₂O₂), a classical model inducer of oxidative stress, and integrated sgRNA constructs were obtained from the cells that survived AFB₁ and H₂O₂ by PCR and Illumina-based sequencing.

Our CRISPR screening identified 94 unique sgRNA sequences, targeting 91 unique protein-coding genes that were present in at least $\sim 0.1\%$ of the total cells analyzed in 3 rounds of AFB₁ exposure (Tables S3–S5). Among the top 0.1% of the most frequently detected sgRNAs, those targeting *BACH1*, *SMARCC1* and *RAB15* were highly enriched in the second round of AFB₁ challenge (Table S4). To reduce the false positive or poorly resistant cells in the early rounds of AFB₁ challenge, we conducted consecutive rounds of selection with increasing concentrations of AFB₁. A comparison of enriched genes from the top 0.1% of hits revealed that 15 targets were common to all 3 rounds of the AFB₁ challenge (Figure 1B). Interestingly, 16 genes were enriched after both AFB₁ exposure and H₂O₂ stimulation, implying that KO of these genes conferred high resistance to both AFB₁- and H₂O₂-induced oxidative stress in these cells (Figure S1A and Table S6). Among the top hits of H₂O₂ selection, *BACH1* emerged as the most significantly enriched (Figure S1B).

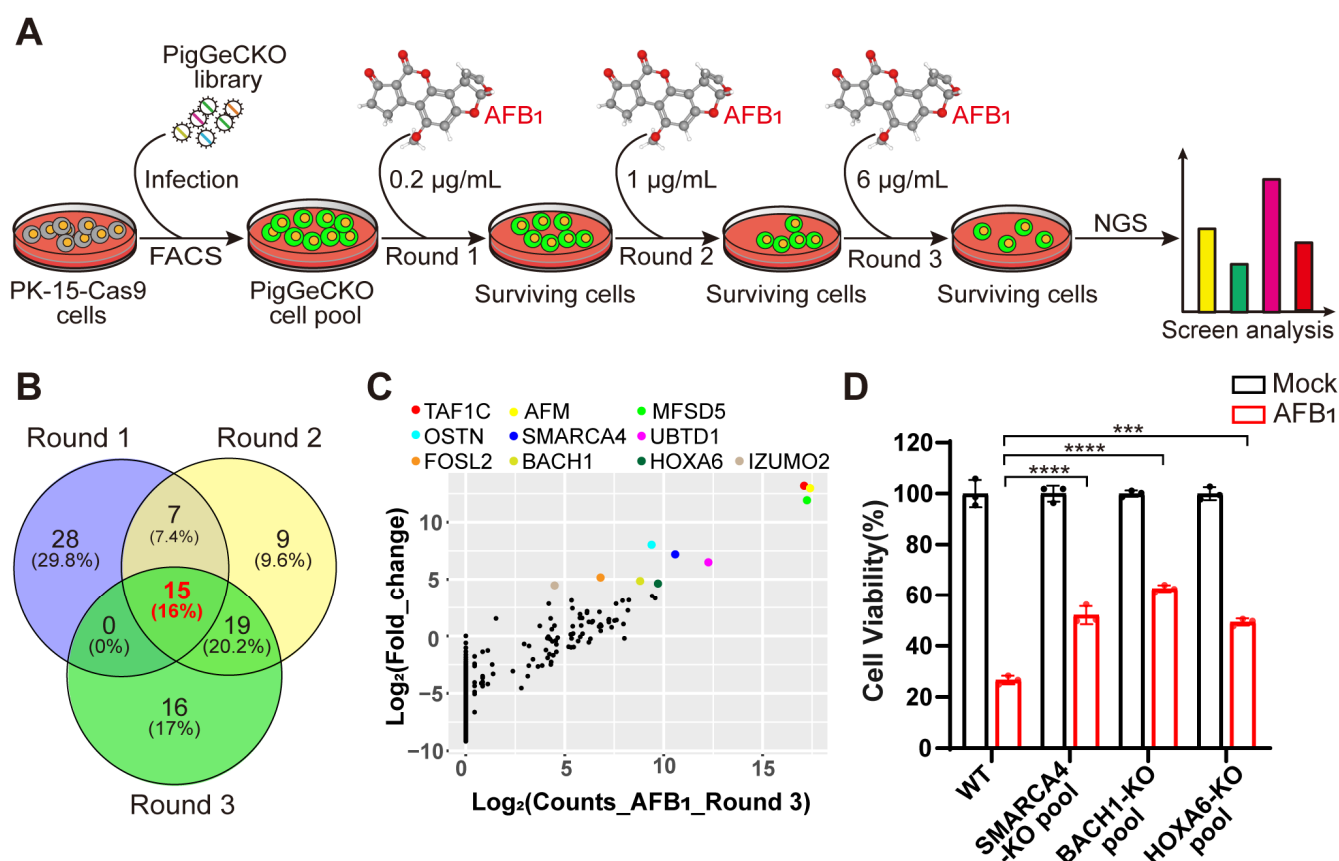


Figure 1. Genome-wide CRISPR/Cas9-based screening to identify genes involved in aflatoxin B₁ toxicity. **(A)** Strategy for CRISPR/Cas9-based aflatoxin B₁ (AFB₁) resistance screening. PK-15 cells expressing Cas9 (PK-15-Cas9) were transduced with a lentiviral PigGeCKO library to generate a pool of mutant cells (PigGeCKO cell pool). Mutant cells were then subjected to sequential rounds of exposure to AFB₁ at increasing concentrations (Round 1: 0.2 µg/mL, Round 2: 1.0 µg/mL, and Round 3: 6.0 µg/mL). AFB₁ was refreshed daily until all control cells were killed. Surviving cells were harvested, and sgRNA sequences were identified by high-throughput sequencing. **(B)** Venn diagram of the top ~0.1% of shared and unique sgRNA target sequences obtained from each round of AFB₁ screening. **(C)** Scatter plots of the frequencies of sgRNA target sequence and the extent of enrichment in transformed PK-15-Cas9 cells in Round 3 of AFB₁ screening. **(D)** Cell viability assays for WT and KO cell pool of candidate genes after AFB₁ exposure at 2 µg/mL for 36 h. *** $p < 0.001$, **** $p < 0.0001$. p values were determined with two-tailed Student's t -tests. AFB₁, aflatoxin B₁; FACS, fluorescence-activated cell sorting; NGS, next-generation sequencing; Round 1 (2 or 3), the first (second or third) round of AFB₁ challenge; WT, wild-type; KO, knockout.

Subsequently, we selected 10 genes that appeared as top hits in Round 3 to test their effects on tolerance to AFB₁ (Figure 1C). Then, utilizing the CRISPR/Cas9 genome-editing system, we created KO mutants for the selected genes in PK-15 cells. Successful disruption of each gene was confirmed by Sanger sequencing (Figure S2). Quantification of AFB₁-induced cell death in heterogeneous pools of three PK-15 KO cells indicated that KO of the gene (i.e., *HOXA6*, *SMARCA4*, *BACH1*) conferred significant resistance to AFB₁-induced cell death, with *BACH1*-deficient cells exhibiting the highest resistance (Figure 1D). Collectively, these results showed that several host factors were involved in AFB₁-induced cell death and that *BACH1* as the greatest outlier played a key role, leading us to select this target for further study.

3.2. BACH1 Is Required for AFB₁-Induced Cell Death

To explore the role of the transcriptional repressor of BACH1 in AFB₁-induced cell death, we isolated a monoclonal BACH1-KO PK-15 cell line (BACH1-KO cells) and confirmed that a +1-bp frameshift mutation in exon 6 resulted in its disruption (Figure S3A). We also confirmed that BACH1 protein was almost completely abolished in the BACH1-KO cells, and that lack of BACH1 had no apparent effect on either cell growth or proliferation (Figures 2A and S3B). Subsequent observation by light microscopy showed that BACH1-KO cells had a near complete resistance to AFB₁, in contrast with WT cells (Figure 2B). Using CCK-8 assays, we calculated the half maximal inhibitory concentration (IC₅₀) of AFB₁ and found that BACH1-KO cells can tolerate remarkably high AFB₁ concentrations, with an IC₅₀ ~8-fold higher than WT cells (Figure 2C). Additionally, since the amino acid sequence of BACH1 is highly conserved amongst pigs and humans (Figure S4), we hypothesized that its function may be conserved across swine and *homo sapiens*. To test this hypothesis, we generated human BACH1-deficient Huh7 cells (hBACH1-KO cells) and confirmed that hBACH1-KO led to significantly higher resistance to AFB₁-induced cell death (Figure S5A,B).

Furthermore, immunofluorescent staining indicated that BACH1-KO cells showed significantly less formation of AFB₁-DNA adducts after AFB₁ exposure compared with WT cells, with approximately 20-fold lower relative fluorescence intensity than WT cells (Figure 2D,E). Through cell-passaging assays, we found that BACH1-KO cells exposed to AFB₁ could be swiftly restored to normal proliferation cycles and cell viability after passaging. In contrast, WT cells exposed to AFB₁ were almost non-viable during passaging, which implied that KO of BACH1 may also confer resistance to AFB₁-induced genotoxicity (Figure S6A,B). Notably, we observed that cells with KO of BACH1 could tolerate multiple mycotoxins, such as AFM₁, AFG₁, and Zearalenone (F-2) (Figure 2F). Taken together, these results indicated that BACH1 functions as an essential mediator of cytotoxicity induced by AFB₁ or other mycotoxins.

3.3. BACH1 Knockout Significantly Alleviates AFB₁-Induced Oxidative Damage by Upregulating Antioxidant Genes

Our findings support that knocking out BACH1, a transcriptional repressor, can lead to the potent inhibition of AFB₁-induced cell death. We sought to identify the BACH1 downstream target genes to determine whether they also participated in AFB₁-induced cell death. RNA sequencing (RNA-Seq) on BACH1-KO and WT cells with and without AFB₁ exposure revealed a total of 2406 DEGs between the AFB₁-treated and untreated cells, 889 DEGs (WT vs. KO), and 1915 DEGs (WT-AFB₁ vs KO-AFB₁) ($|\log_2(\text{FoldChange})| \leq 2$ and p value ≤ 0.001) (Figure S7A–C, Tables S7–S9). GSEA indicated that BACH1-depleted cells exhibited enhanced expressions of genes involved in oxidation–reduction processes compared with the WT cells (Figure 3A). Heatmap visualization of the core set of enriched DEGs from GSEA revealed a trend of significant upregulation among antioxidant genes in both WT and BACH1-KO cells after 36 h exposure to AFB₁ (Figure 3B). The STRING database was next used to construct a DEG PPI network, and the core genes from GSEA with the highest values were determined using Cytoscape v. 3.7.2, which showed that knocking out BACH1 could affect the expression of multiple downstream genes involved in oxidation reduction (Figure S8).

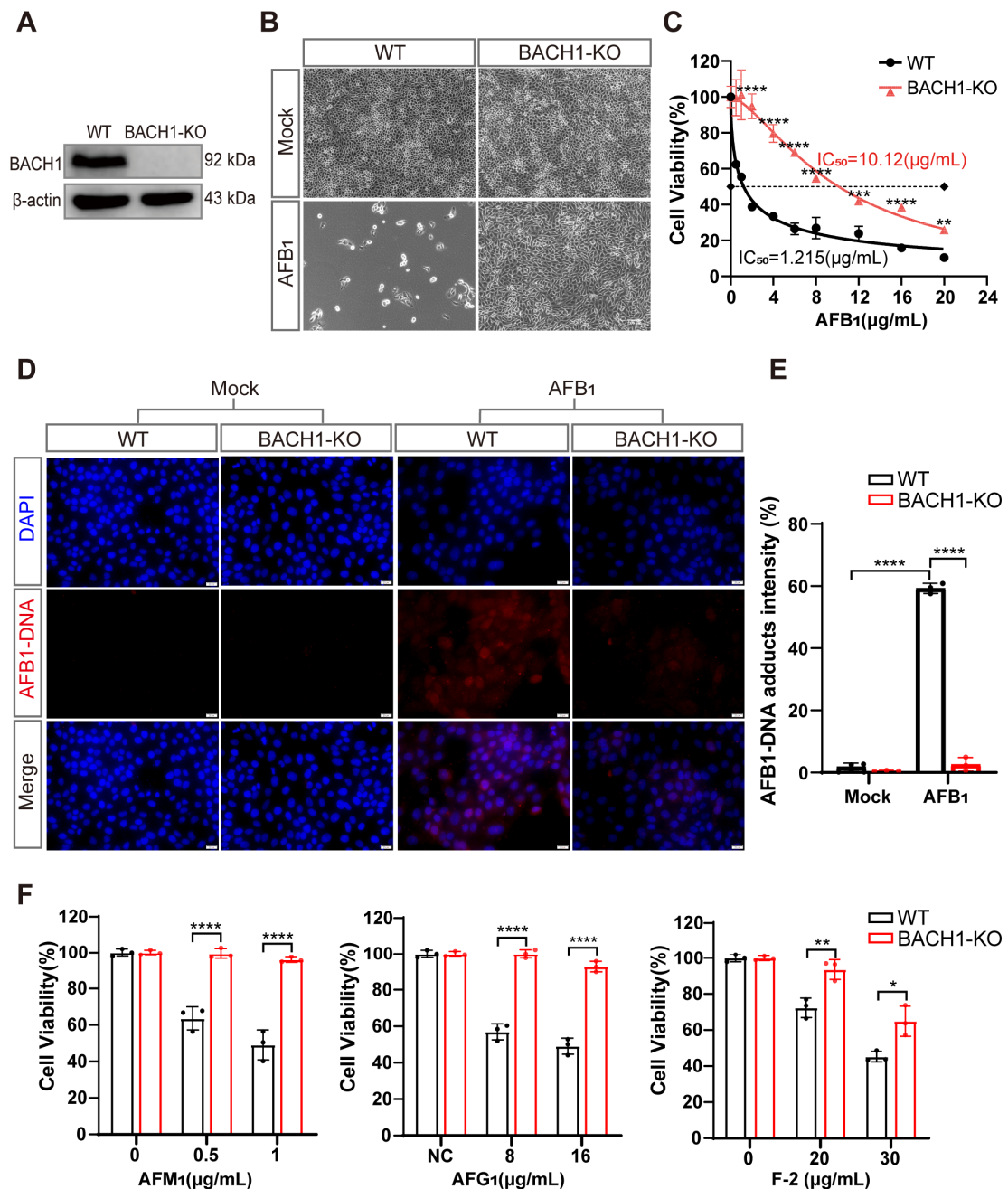


Figure 2. BACH1 knockout cells exhibit higher resistance to aflatoxin B₁. (A) Western blot analysis of BACH1 expression in WT and KO cells. (B) Representative images of WT and BACH1-KO PK-15 cells challenged with 2 $\mu\text{g/mL}$ AFB₁ for 48 h. Scale bar, 100 μM . (C) The IC_{50} values for AFB₁ in WT and BACH1-KO cells determined by CCK-8 assays. (D,E) Immunofluorescence staining of AFB₁-induced DNA adduct formation in WT and BACH1-KO cells; relative fluorescence intensity calculated using ImageJ software. Scale bar, 20 μM . (F) Enhanced resistance to AFM₁, AFG₁, and F-2 in BACH1-KO cells. WT and BACH1-KO cells were treated with AFM₁ (at 0.5 $\mu\text{g/mL}$ and 1 $\mu\text{g/mL}$), AFG₁ (at 8 $\mu\text{g/mL}$ and 10 $\mu\text{g/mL}$), and F-2 (at 20 $\mu\text{g/mL}$ and 30 $\mu\text{g/mL}$) for 36 h. Cell viability was measured with CCK-8 assays. * $p < 0.05$, ** $p < 0.01$, *** $p < 0.001$, **** $p < 0.0001$. p values were determined with two-tailed Student's t -tests. AFB₁, aflatoxin B₁; AFG₁, aflatoxin G₁; F2, zearalenone; WT, wild-type; KO, knockout.

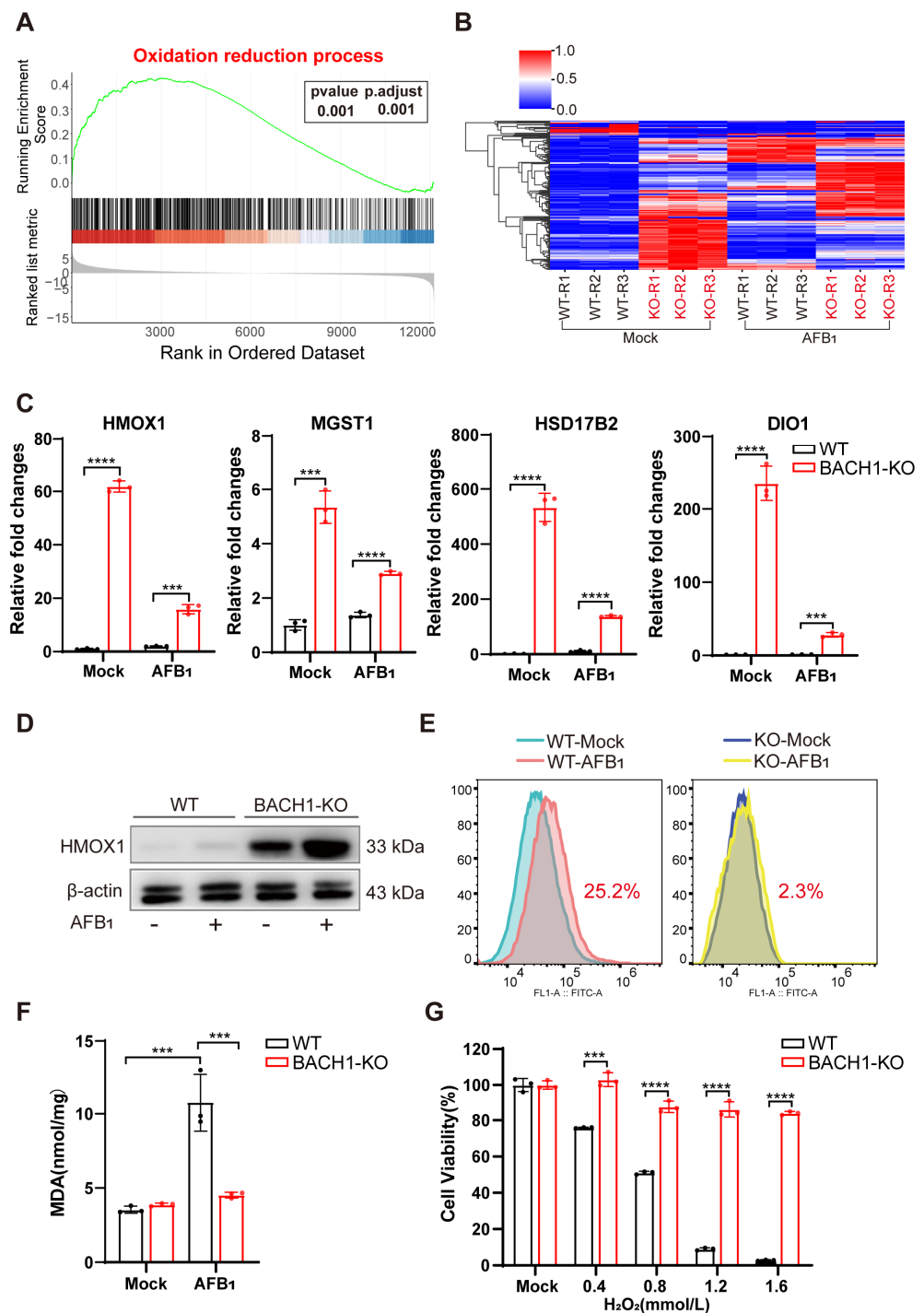


Figure 3. BACH1 deficiency attenuates oxidative damage from AFB₁ via upregulation of antioxidant factors. (A) Gene set enrichment analysis (GSEA) identified the oxidation–reduction process as significantly enriched with differentially upregulated genes in RNA-Seq data of BACH1-KO cells treated with AFB₁. (B) Heatmap of the relative expression levels of genes in the core enrichment subset of GSEA. (C) qPCR validation of RNA-Seq data showing differential mRNA expression of antioxidant genes in oxidation reduction. (D) Western blot analysis of HMOX1 in WT and BACH1-KO cells with and without AFB₁ exposure. (E) BACH1-KO cells exhibit lower levels of AFB₁-induced ROS. (F) Comparison of MDA levels induced by AFB₁ in WT and BACH1-KO cells. (G) H₂O₂-induced cell death in WT and BACH1-KO cells. *** $p < 0.001$, **** $p < 0.0001$. p values were determined with two-tailed Student's t -tests. AFB₁, aflatoxin B₁; WT, wild-type; KO, knockout; RT-qPCR, Real-time quantitative PCR.

Among these AFB₁-inducible antioxidant genes, the mRNA expression of *HMOX1*, *MGST1*, *HSD17B2*, and *DIO1*, were upregulated in BACH1-KO cells with and without AFB₁ exposure (Figures 3C and S9). In addition, Western blot analysis confirmed that HMOX1 protein levels were also obviously upregulated in BACH1-KO, but not with WT cells, regardless of their exposure to AFB₁ (Figure 3D). The results indicated that KO of BACH1 mitigated the inhibition of these antioxidant genes. To test the effects of this inhibition, we quantified ROS and MDA content, the markers of oxidative stress and lipid peroxidation, using DCFH-DA assay and TBARS assay, respectively. The results showed that ROS production was induced by AFB₁ in WT cells and that this production was significantly reduced (i.e., from 22.5% to 2.3%) in BACH1-KO cells (Figure 3E). Furthermore, BACH1 KO also resulted in decreased levels of MDA in response to AFB₁ (Figure 3F) and significantly inhibited cell death induced by H₂O₂, indicating that these BACH1-KO cells displayed a high antioxidant capacity. Taken together, these results demonstrated that BACH1 deficiency can reduce AFB₁-induced oxidative damage by activating the expression of antioxidant factors, thus alleviating cytotoxicity.

3.4. Identifying Inhibitors of AFB₁-Induced Cell Death That Target BACH1

To identify novel potential inhibitors that confer high resistance to AFB₁ exposure, we conducted structure-based virtual screening targeting BACH1 using the known structure of human BACH1 protein obtained from the PDB database. We used the Specs small-molecule compound database of 55,024 compounds as the ligand library for virtual docking with human BACH1 (Figure 4A). Ranking the predicted activity scores revealed that compounds M1, M2, and M3 exhibited strong binding energy interacting with hBACH1 (Figures 4A and S10A; abbreviations of and synonyms for M1, M2, and M3 are listed in Table S2). The treatment of Huh7 cells with 10 µg/mL of each compound showed that only exposure to M2 resulted in any significant inhibition of AFB₁-induced cell death (Figure 4B). Furthermore, M2 did not affect the cell proliferation in cytotoxicity assays, suggesting that it has no obvious toxic effects on cells (Figure S10B). Subsequently, we found that M2 treatment could also protect cells under increasingly high concentrations of AFB₁ in Huh7 cells (Figure 4C). To further study the effects of this inhibitor on cellular resistance to AFB₁, we quantified the levels of AFB₁-DNA adducts in Huh7 cells exposed to AFB₁. The results indicated that M2-treated cells had reduced formations of AFB₁-DNA adducts, with approximately fifteen-fold lower relative fluorescence intensity than control cells (Figure 4D).

Molecular docking and dynamic simulation of M2 on the surface of human BACH1 revealed the three amino acid residues (Ser-13, Ser-14, and Ser-17) with the lowest binding energy (2.0, 1.9, and 2.4 kcal/mol, respectively), suggesting that these residues were candidate binding sites for M2 (Figure S11A). Given the high level of conservation between human and pig BACH1 (Figure S4), we then explored these potential M2 docking loci (Ser-13, Ser-14, and Ser-17) in porcine BACH1. Sequence alignments confirmed that these residues were highly conserved (Figure S11B), which led us to test the effects of M2 in PK-15 cells. We found that M2 treatment could also confer resistance to AFB₁-induced cell death in porcine cells (Figure 4E). Further IC₅₀ assays indicated that AFB₁ resistance was enhanced by over threefold in the presence of M2 (Figure 4F), while the formation of AFB₁-DNA adducts was significantly reduced by M2 treatment in PK-15 cells (Figure 4G).

We next sought to determine whether other small-molecule inhibitors with a similar structure to M2 could similarly affect the cellular response to AFB₁. We speculated that the 1,3-benzodioxin functional moieties at M2 may play a central role in mediating resistance to AFB₁ (Figure S10A). We then selected 182 compounds with >70% similarity to M2 from the Specs small-molecule compound database. Using a virtual screening strategy, six M2 analogues, designated as M4, M5, M6, M7, M8, and M9, were chosen as candidates (Figure S12A, Table S2). Further cell viability assays showed that treatment with five of the six analogues resulted in lower AFB₁-induced cell death in Huh7 cells, while only three

analogues led to lower cell death from AFB₁ in PK-15 cells (Figure S12B,C). These results suggested that the same inhibitors have different effects on AFB₁ toxicity through BACH1 in different species. However, our overall results showed that M2 targeting of BACH1 resulted in significant resistance to AFB₁ exposure in both human and porcine cells.

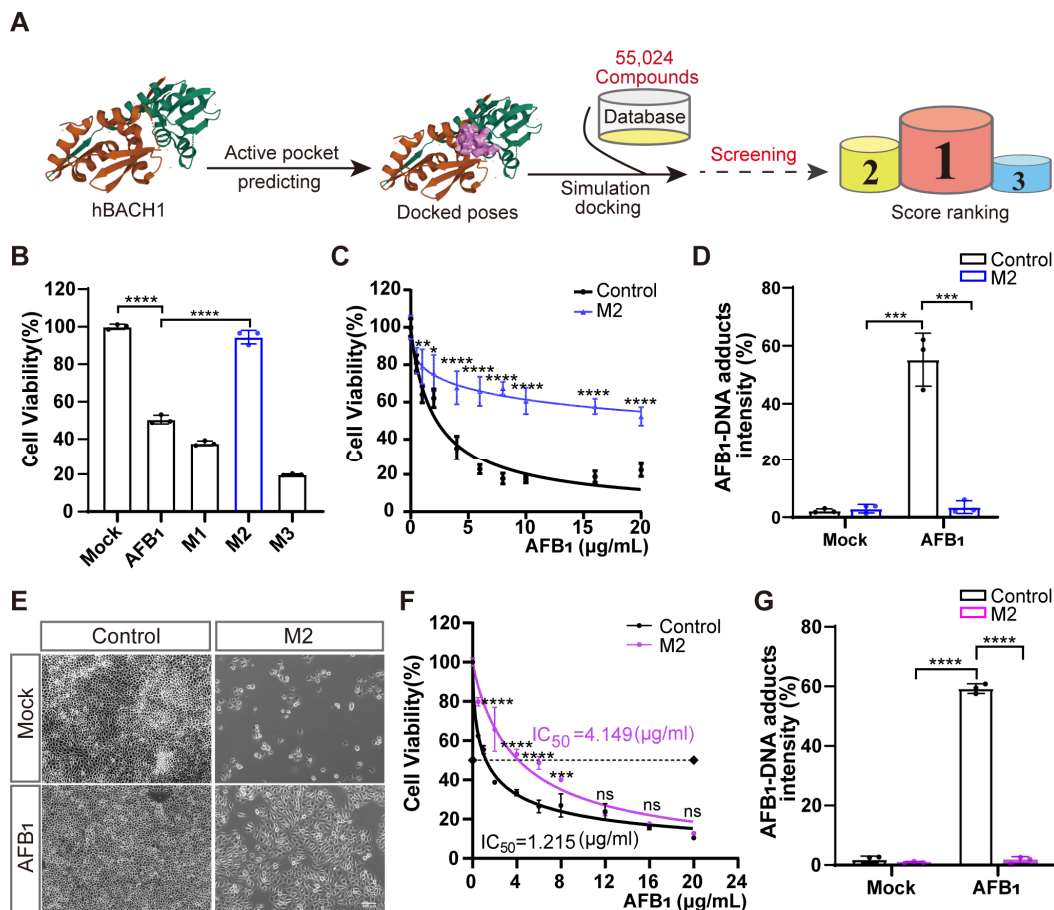


Figure 4. Treatment with inhibitor M2 leads to the highest resistance to aflatoxin B₁ in vitro. (A) Workflow of the structure-based virtual screening to identify inhibitors targeting BACH1. (B) Validation of the top three inhibitors (M1, M2, and M3) in Huh7 cells by CCK-8 assays. (C) Comparison of Huh7 tolerance to different AFB₁ concentrations with and without M2 treatment. (D) The relative fluorescence intensity of AFB₁-DNA adducts in Huh7 cells with and without M2 treatment. (E) Representative light microscopy images of AFB₁-treated PK-15 cells with or without M2 treatment. Scale bar, 100 µm. (F) The IC₅₀ assays for AFB₁ in PK-15 cells with and without M2 treatment determined with CCK-8 assays. (G) The relative fluorescence intensity of AFB₁-DNA adducts in PK-15 cells with and without M2 treatment. * $p < 0.05$, ** $p < 0.01$, *** $p < 0.001$, **** $p < 0.0001$, ns, not significant. p values were determined with two-tailed Student's t -tests. AFB₁, aflatoxin B₁; M1, 1-Piperazineethanol, 4-phenyl- α -[(3,4,5-trimethoxyphenyl)methoxy]methyl]; M2, 1-Piperazineethanol, α -[(1,3-benzodioxol-5-yloxy)methyl]-4-(2-methoxyphenyl); M3, 1,2-Ethanediamine, N1, N1, N2, N2-tetrakis (1H-benzimidazol-2-ylmethyl).

3.5. BACH1 Inhibitor Reduces the AFB₁-Induced Liver Damage In Vivo

Given the above findings that the predicted docking locus was conserved between pigs and humans, and that M2 could mitigate the effects of AFB₁ in both porcine and human cells, we investigated the effects of the BACH1 inhibitor M2 during exposure to AFB₁ in vivo. To this end, we challenged healthy SD rats with AFB₁ with and without M2 treatment (Figure S13). The overall workflow for M2 treatment assays is illustrated in Figure 5A. Briefly, healthy rats were treated with AFB₁ with or without M2 or with M2 alone by intraperitoneal injection for three days. After challenge with AFB₁ rats, were given a 7-day recovery period. We observed that the body weights of rats treated with AFB₁ + M2

were higher than those of rats given AFB₁ alone, while M2 alone at 20 mg/kg showed no cytotoxicity in rats (Figure 5B). In addition, comparisons of liver pathological tissue slices showed that symptoms of hepatocellular edema and inflammatory cell infiltration in the liver tissue caused by AFB₁ exposure were effectively alleviated in rats treated with M2 (Figure 5C). Similarly, immunohistochemical staining of liver tissues to detect the formation of AFB₁-DNA adducts indicated that adduct levels were lower in rats in the AFB₁ + M2 treatment group (Figure 5D). Moreover, M2 treatment was associated with lower AFB₁-induced MDA production in liver tissue, which implied that M2 might alleviate AFB₁-induced liver damage by decreasing oxidative stress (Figure 5E). Taken together, these results indicated that BACH1 could serve as an effective target for the treatment of oxidative damage induced by AFB₁, while the M2 inhibitor of BACH1 could reduce AFB₁-induced liver damage (Figure 5F).

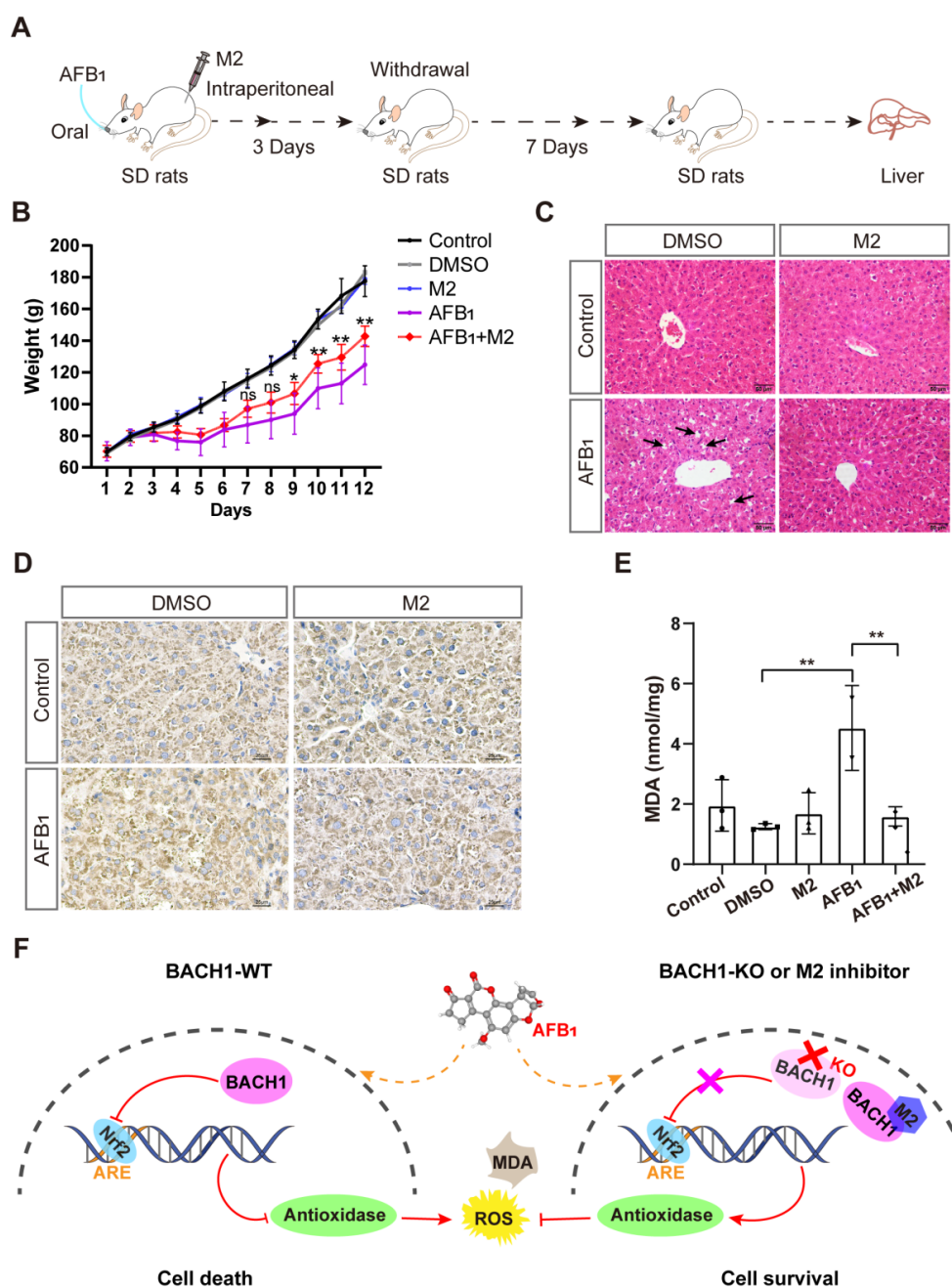


Figure 5. Liver damage from aflatoxin B₁ is significantly lower in M2-treated rats. (A) Schematic of M2 treatment of AFB₁-induced SD rats. (B) Body weights of SD rats during AFB₁ exposure with and

without M2 treatment. (C) Liver histopathology of AFB₁-exposed rats and control group. The specific inflammatory cell infiltration is indicated with an arrow. Scale bar, 50 μ m. (D) Representative light microscopy images of immunohistochemical staining for AFB₁-DNA adducts in liver tissues with and without M2 treatment. Scale bar, 25 μ m. (E) MDA levels in liver tissues with and without M2 treatment. (F) Proposed molecular model of BACH1 and M2 in AFB₁-exposed cells. * $p < 0.05$, ** $p < 0.01$, ns, not significant. p values were determined with two-tailed Students' t -tests. ROS, reactive oxygen species; MDA, malondialdehyde; AFB₁, aflatoxin B₁; WT, wild-type; KO, knockout; DMSO, dimethyl sulfoxide; DMSO used as a negative control; Nrf2, NF-E2-related factor 2; ARE, antioxidant response element; M2, 1-Piperazineethanol, α -[(1,3-benzodioxol-5-yloxy)methyl]-4-(2-methoxyphenyl); SD rats, Sprague-Dawley (SD) rats.

4. Discussion

Aflatoxin B₁ (AFB₁) and its metabolites (e.g., AFM₁) can accumulate in animal tissues and be assimilated through human consumption of animal products. AFB₁ toxicity in livestock and humans can lead to adverse economic losses accompanied by serious health concerns. Determining host factors required for AFB₁ toxicity and revealing their molecular mechanisms is essential for resolving aflatoxicosis through developing novel therapeutic targets and through the targeted breeding of AFB₁-resistant livestock, such as swine. We executed a genome-wide CRISPR/Cas9 KO screening in PK-15 cells and identified several host factors potentially related to the toxic effects of AFB₁. Among the top candidates, the transcriptional repressor BACH1 was the most significant target of AFB₁. We subsequently characterized BACH1 as a central mediator of AFB₁-induced oxidative damage. Furthermore, using a structure-based virtual screening strategy, we developed a small-molecule inhibitor (M2) that attenuates AFB₁ toxicity via targeting BACH1.

BACH1 regulates the genes involved in mitotic chromatin dynamics, apoptosis, oxidative stress response, and cell cycle [26]. However, no studies have yet reported the link between AFB₁ and the molecular mechanism of BACH1 in AFB₁ toxicity. We conducted an RNA-Seq analysis to uncover the gene regulatory network relevant to AFB₁ toxicity and found significant enrichment for differentially upregulated genes involved in the oxidation–reduction process in BACH1-KO cells. Other studies have reported that AFB₁ negatively affects the balance between antioxidants and pro-oxidants, resulting in elevated lipid peroxidation and oxidative damage [23,27]. Oxidative stress is associated with multiple disorders such as cancers, atherosclerosis, and Alzheimer's disease [28]. Our results showed reduced ROS and MDA in BACH1 KO cells with an increased expression of antioxidant genes such as *HMOX1* and *MGST1* (Figure 5F). Therefore, BACH1 is a crucial factor in AFB₁-induced oxidative damage by regulating the expression of antioxidant genes.

Currently, reports on BACH1 inhibitors are limited, with little or no information on their characterization and outcomes on AFB₁ resistance [29–31]. Structure-based virtual screening has several advantages in identifying potential inhibitors of specific genes, such as reduced time constraints, cost-effectiveness, and higher throughput than the conventional screening of drug panels [32]. Using a structure-based virtual screening approach, we developed several inhibitors that effectively decreased AFB₁ toxicity by targeting BACH1. Although M1 has a similar backbone to M2, M1 lacks the 1,3-benzodioxin functional moieties and has no resistance to AFB₁ toxicity (Figures 4B and S10A). Therefore, the 1,3-benzodioxin functional moieties at the chemical structure of M2 may play a central role in inhibiting AFB₁ toxicity. We selected six other inhibitors with similar conformations to M2 and tested their effects on AFB₁ resistance. In human cells, M4, M5, M6, M7, and M8 exhibited anti-AFB₁ effects (Figure S12B). Structural analyses of these compounds revealed a 1,3-benzodioxin structure. Specifically, M4, M5, and M6 contain tertiary amine positive ions and elicit enhanced anti-AFB₁ effects compared with M7 and M8 (Figure S12A,B). The phenyl or benzyloxy moieties of M5, M6, and M8 may endow the tertiary amine cation with stronger electrophilicity and enhance the polarity of the compounds with increased protein-binding capacity. In addition, we found that the same inhibitors lead to increased resistance to AFB₁ in human cells than in porcine cells (Figure S12B,C). We used the human BACH1

structure to conduct virtual screening since the porcine BACH1 structure is unknown. This likely explains why the inhibitors conferred higher AFB₁ resistance in human cells than in porcine cells. We, therefore, suppose that the protein structure of BACH1 may differ slightly between humans and pigs, even though the essential BACH1 binding amino acids for M2 (Ser-13, Ser-14, and Ser-17) were conserved in both species. Overall, BACH1 is a potential druggable target for AFB₁ (Figure 5F). Further investigations are warranted for comprehensively characterizing BACH1 and M2 interactions.

Finally, we found that an M2 inhibitor can attenuate AFB₁ toxicity in rats. Since we confirmed that M2 is effective in cells with acute exposure to AFB₁, SD rats were used to establish an in vivo model for oxidative damage induced by acute AFB₁ exposure. The results indicated that treatment with M2 reduces the formation of AFB₁-DNA adducts and MDA in liver tissue, thus alleviating liver damage. AFB₁ is hepatotoxic and is a significant factor in promoting the development of primary hepatocellular carcinoma (HCC) [5]. Moreover, other studies reported that BACH1 is upregulated in HCC samples, with BACH1 facilitating the growth and metastasis of HCC [33,34]. Therefore, we hypothesize that M2 may be effective in treating HCC, although further studies are needed to confirm this possibility.

5. Conclusions

In summary, we identified BACH1 as a novel host factor mediating AFB₁ toxicity. BACH1-deficient cells can tolerate high concentrations of AFB₁ by increasing the expression of antioxidant genes. Additionally, the inhibitor M2, which targets BACH1, can provide strong resistance to AFB₁ toxicity in vitro and in vivo, suggesting its potential for clinical development as a therapeutic intervention against AFB₁ toxicity.

Supplementary Materials: The following supporting information can be downloaded at: <https://www.mdpi.com/article/10.3390/antiox11091787/s1>; Figure S1: The surviving cells in the second round were challenged with H₂O₂, Figure S2: Sanger sequencing of mutants aligned to reference sequences for *HOXA6*, *SMARCA4*, and *BACH1*, Figure S3: Construction of single-clone-originated *BACH1* knockout PK-15 cells, Figure S4: Alignment of the amino acid sequences of BACH1 between pig and human, Figure S5: Confirmed resistance to AFB₁ in Huh7 cells, Figure S6: Exploration of the tolerance to AFB₁ in WT and BACH1-KO cells with cell-passaging assays, Figure S7: Volcano map of differentially expressed genes (DEGs), Figure S8: Protein–protein interaction (PPI) network of the core genes from GSEA was visualized by Cytoscape (wild-type vs knockout), Figure S9: The mRNA expression of antioxidant genes in oxidation reduction process was tested with RT-qPCR, Figure S10: The inhibitors from the structure-based virtual screening, Figure S11: The analysis of the structure of human and pig BACH1, Figure S12: Other inhibitors with similar structures to M2, Figure S13: Alignment of the amino acid sequences of BACH1 from human and rat, Table S1: Primer pairs and sgRNA-targeting sequences used in this study, Table S2: Inhibitors used in this study, Table S3: Sequencing results for the top ~0.1% of sgRNA (PigGeCKO) in the first round of AFB₁ screens after challenge, Table S4: Sequencing results for the top ~0.1% of sgRNA (PigGeCKO) in the second round of AFB₁ screens after challenge, Table S5: Sequencing results for the top ~0.1% of sgRNA (PigGeCKO) in the third round of AFB₁ screens after challenge, Table S6: Sequencing results for the top ~0.1% of sgRNA (PigGeCKO) in H₂O₂ screens after challenge, Table S7: Differential gene expression analysis between PK-15 cells (WT) and BACH1-KO cells by RNA-Seq, Table S8: Differential gene expression analysis between untreated PK-15 cells and AFB₁-treated PK-15 cells by RNA-Seq, Table S9: Differential gene expression analysis between AFB₁-treated PK-15 cells (WT) and AFB₁-treated BACH1-KO cells by RNA-Seq.

Author Contributions: Most of the experimental work was co-conducted by J.Z. and S.H., with minor contributions from C.Z., Y.Z., L.Z., H.L., P.Z., S.L., L.F., Z.Z., Y.X., X.X., J.R., X.L., L.S. and G.C., S.Z., X.W. and S.X. conceived the project and designed the experiments. J.Z., S.H. and S.X. wrote the manuscript. X.W. helped in revising the manuscript. All authors contributed to manuscript revision. All authors have read and agreed to the published version of the manuscript.

Funding: This work was supported by the Laboratory of Lingnan Modern Agriculture Project (No. NZ2021005), the Natural Science Foundation of China (No. 32072685), the Fund of Modern Industrial Technology System of Pig (CARS-35), the Major Project of Hubei Hongshan Laboratory (2021hszd003), and the Key Research and Development Program of Guangxi (AB19245030).

Institutional Review Board Statement: The animal study protocol was approved by the Tab of Animal Experimental Ethical Inspection of Laboratory Animal Centre, Huazhong Agriculture University (HZAURA-2022-0004).

Informed Consent Statement: Not applicable.

Data Availability Statement: The deep-sequencing and RNA-Seq data generated in this study have been deposited and are available in the GEO database under accessions GSE199384 and GSE199385, respectively. Additional data related to this paper may be requested from the authors.

Acknowledgments: The authors would like to thank Limeng Sun for providing experimental materials; Xingxu Huang and Hao Wu for helpful comments; Emmanuel Mulaya Khazalwa for language editing assistance during the preparation of this manuscript; Yan Wang (Institute of Hydrobiology, Chinese Academy of Sciences) for her assistance with flow cytometry. We thank the public technology service platform of Key Laboratory of Agricultural Animal Genetics, Breeding and Reproduction (Ministry of Education) for assistance in lentivirus purification, and we would be grateful to Jing Xu for her support of sample preparation, data acquisition and analysis.

Conflicts of Interest: The authors declare no conflict of interest.

References

1. Klich, M.A. *Aspergillus flavus*: The major producer of aflatoxin. *Mol. Plant Pathol.* **2007**, *8*, 713–722. [[CrossRef](#)] [[PubMed](#)]
2. Yabe, K.; Ando, Y.; Hamasaki, T. Biosynthetic relationship among aflatoxins B₁, B₂, G₁, and G₂. *Appl. Environ. Microbiol.* **1988**, *54*, 2101–2106. [[CrossRef](#)] [[PubMed](#)]
3. Huang, W.; Cao, Z.; Yao, Q.; Ji, Q.; Zhang, J.; Li, Y. Mitochondrial damage are involved in Aflatoxin B₁-induced testicular damage and spermatogenesis disorder in mice. *Sci. Total Environ.* **2020**, *701*, 135077. [[CrossRef](#)] [[PubMed](#)]
4. Rushing, B.R.; Selim, M.I. Aflatoxin B₁: A review on metabolism, toxicity, occurrence in food, occupational exposure, and detoxification methods. *Food Chem. Toxicol.* **2019**, *124*, 81–100. [[CrossRef](#)]
5. Ren, X.L.; Han, P.; Meng, Y. Aflatoxin B₁-Induced COX-2 Expression Promotes Mitophagy and Contributes to Lipid Accumulation in Hepatocytes In Vitro and In Vivo. *Int. J. Toxicol.* **2020**, *39*, 594–604. [[CrossRef](#)] [[PubMed](#)]
6. Shin, K.; Guo, J.; Niu, Y.; Cui, X. The toxic effect of aflatoxin B₁ on early porcine embryonic development. *Theriogenology* **2018**, *118*, 157–163. [[CrossRef](#)]
7. Chu, Y.J.; Yang, H.I.; Wu, H.C.; Liu, J.; Wang, L.Y.; Lu, S.N.; Lee, M.H.; Jen, C.L.; You, S.L.; Santella, R.M.; et al. Aflatoxin B₁ exposure increases the risk of cirrhosis and hepatocellular carcinoma in chronic hepatitis B virus carriers. *Int. J. Cancer* **2017**, *141*, 711–720. [[CrossRef](#)] [[PubMed](#)]
8. Lei, M.; Zhang, N.; Qi, D. In vitro investigation of individual and combined cytotoxic effects of aflatoxin B₁ and other selected mycotoxins on the cell line porcine kidney 15. *Exp. Toxicol. Pathol.* **2013**, *65*, 1149–1157. [[CrossRef](#)]
9. Hou, L.; Zhou, X.; Gan, F.; Liu, Z.; Zhou, Y.; Qian, G.; Huang, K. Combination of Selenomethionine and N-Acetylcysteine Alleviates the Joint Toxicities of Aflatoxin B₁ and Ochratoxin A by ERK MAPK Signal Pathway in Porcine Alveolar Macrophages. *J. Agric. Food Chem.* **2018**, *66*, 5913–5923. [[CrossRef](#)]
10. Pang, V.F.; Chiang, C.F.; Chang, C.C. The in vitro effects of aflatoxin B₁ on physiological functions of swine alveolar macrophages. *Vet. Med. Sci.* **2020**, *6*, 919–925. [[CrossRef](#)]
11. Cao, Q.Q.; Lin, L.X.; Xu, T.T.; Lu, Y.; Zhang, C.D.; Yue, K.; Huang, S.C.; Dong, H.J.; Jian, F.C. Aflatoxin B₁ alters meat quality associated with oxidative stress, inflammation, and gut-microbiota in sheep. *Ecotoxicol. Environ. Saf.* **2021**, *225*, 112754. [[CrossRef](#)] [[PubMed](#)]
12. Grosu, I.A.; Pistol, G.C.; Taranu, I.; Marin, D.E. The Impact of Dietary Grape Seed Meal on Healthy and Aflatoxin B₁ Afflicted Microbiota of Pigs after Weaning. *Toxins* **2019**, *11*, 25. [[CrossRef](#)] [[PubMed](#)]
13. Verheecke, C.; Liboz, T.; Mathieu, F. Microbial degradation of aflatoxin B₁: Current status and future advances. *Int. J. Food Microbiol.* **2016**, *237*, 1–9. [[CrossRef](#)] [[PubMed](#)]
14. Proudfoot, C.; Mcfarlane, G.; Whitelaw, B.; Lillico, S. Livestock breeding for the 21st century: The promise of the editing revolution. *Front. Agric. Sci. Eng.* **2020**, *7*, 129. [[CrossRef](#)]
15. Wang, H.; Wu, S.; Capocchi, M.R.; Jaenisch, R. A brief review of genome editing technology for generating animal models. *Front. Agric. Sci. Eng.* **2020**, *7*, 123. [[CrossRef](#)]
16. Lou, A.G.; Cai, J.S.; Zhang, X.M.; Cui, C.D.; Piao, Y.S.; Guan, L.Z. The aflatoxin-detoxifyzyme specific expression in the parotid gland of transgenic pigs. *Transgenic Res.* **2017**, *26*, 677–687. [[CrossRef](#)]

17. Umayya, S.R.; Vijayalakshmi, Y.C.; Sejian, V. Exploration of plant products and phytochemicals against aflatoxin toxicity in broiler chicken production: Present status. *Toxicon* **2021**, *200*, 55–68. [[CrossRef](#)]
18. Deng, J.; Zhao, L.; Zhang, N.; Karrow, N.A.; Krumm, C.S.; Qi, D.; Sun, L. Aflatoxin B1 metabolism: Regulation by phase I and II metabolizing enzymes and chemoprotective agents. *Mutat. Research. Rev. Mutat. Res.* **2018**, *778*, 79–89. [[CrossRef](#)]
19. Pauletto, M.; Giantin, M.; Tolosi, R.; Bassan, I.; Barbarossa, A.; Zaghini, A.; Dacasto, M. Curcumin Mitigates AFB1-Induced Hepatic Toxicity by Triggering Cattle Antioxidant and Anti-Inflammatory Pathways: A Whole Transcriptomic In Vitro Study. *Antioxidants* **2020**, *9*, 1059. [[CrossRef](#)]
20. Lee, H.S.; Lindahl, J.; Nguyen-Viet, H.; Khong, N.V.; Nghia, V.B.; Xuan, H.N.; Grace, D. An investigation into aflatoxin M 1 in slaughtered fattening pigs and awareness of aflatoxins in Vietnam. *BMC Vet. Res.* **2017**, *13*, 363. [[CrossRef](#)]
21. Zhu, Q.; Ma, Y.; Liang, J.; Wei, Z.; Li, M.; Zhang, Y.; Liu, M.; He, H.; Qu, C.; Cai, J.; et al. AHR mediates the aflatoxin B1 toxicity associated with hepatocellular carcinoma. *Signal Transduct. Target. Ther.* **2021**, *6*, 299. [[CrossRef](#)] [[PubMed](#)]
22. Jeschke, U.; Zhang, X.; Kuhn, C.; Jalaguier, S.; Colinge, J.; Pfender, K.; Mayr, D.; Ditsch, N.; Harbeck, N.; Mahner, S.; et al. The Prognostic Impact of the Aryl Hydrocarbon Receptor (AhR) in Primary Breast Cancer Depends on the Lymph Node Status. *Int. J. Mol. Sci.* **2019**, *20*, 106. [[CrossRef](#)]
23. Xu, Q.; Shi, W.; Lv, P.; Meng, W.; Mao, G.; Gong, C.; Chen, Y.; Wei, Y.; He, X.; Zhao, J.; et al. Critical role of caveolin-1 in aflatoxin B1-induced hepatotoxicity via the regulation of oxidation and autophagy. *Cell Death Dis.* **2020**, *11*, 6. [[CrossRef](#)] [[PubMed](#)]
24. Zhao, C.; Liu, H.; Xiao, T.; Wang, Z.; Nie, X.; Li, X.; Qian, P.; Qin, L.; Han, X.; Zhang, J.; et al. CRISPR screening of porcine sgRNA library identifies host factors associated with Japanese encephalitis virus replication. *Nat. Commun.* **2020**, *11*, 5178. [[CrossRef](#)]
25. Wang, X.; He, Y.; Tian, J.; Muhammad, I.; Liu, M.; Wu, C.; Xu, C.; Zhang, X. Ferulic acid prevents aflatoxin B1-induced liver injury in rats via inhibiting cytochrome P450 enzyme, activating Nrf2/GST pathway and regulating mitochondrial pathway. *Ecotox. Environ. Safe.* **2021**, *224*, 112624. [[CrossRef](#)] [[PubMed](#)]
26. Wang, X.; Liu, J.; Jiang, L.; Wei, X.; Niu, C.; Wang, R.; Zhang, J.; Meng, D.; Yao, K. Bach1 Induces Endothelial Cell Apoptosis and Cell-Cycle Arrest through ROS Generation. *Oxid. Med. Cell. Longev.* **2016**, *2016*, 6234043. [[CrossRef](#)] [[PubMed](#)]
27. Liu, Y.; Wang, W. Aflatoxin B1 impairs mitochondrial functions, activates ROS generation, induces apoptosis and involves Nrf2 signal pathway in primary broiler hepatocytes. *Anim. Sci. J.* **2016**, *87*, 1490–1500. [[CrossRef](#)]
28. Forman, H.J.; Zhang, H. Targeting oxidative stress in disease: Promise and limitations of antioxidant therapy. *Nat. Rev. Drug Discov.* **2021**, *20*, 689–709. [[CrossRef](#)]
29. Casares, L.; Garcia, V.; Garrido-Rodriguez, M.; Millan, E.; Collado, J.A.; Garcia-Martin, A.; Penarando, J.; Calzado, M.A.; de la Vega, L.; Munoz, E. Cannabidiol induces antioxidant pathways in keratinocytes by targeting BACH1. *Redox Biol.* **2020**, *28*, 101321. [[CrossRef](#)]
30. Attucks, O.C.; Jasmer, K.J.; Hannink, M.; Kassis, J.; Zhong, Z.; Gupta, S.; Victory, S.F.; Guzel, M.; Poliseti, D.R.; Andrews, R.; et al. Induction of heme oxygenase I (HMOX1) by HPP-4382: A novel modulator of Bach1 activity. *PLoS ONE* **2014**, *9*, e101044. [[CrossRef](#)]
31. Casares, L.; Unciti-Broceta, J.D.; Prados, M.E.; Caprioglio, D.; Mattoteia, D.; Higgins, M.; Apendino, G.; Dinkova-Kostova, A.T.; Munoz, E.; de la Vega, L. Isomeric O-methyl cannabidiolquinones with dual BACH1/NRF2 activity. *Redox Biol.* **2020**, *37*, 101689. [[CrossRef](#)] [[PubMed](#)]
32. Odhar, H.A.; Ahjel, S.W.; Albeer, A.; Hashim, A.F.; Rayshan, A.M.; Humadi, S.S. Molecular docking and dynamics simulation of FDA approved drugs with the main protease from 2019 novel coronavirus. *Bioinformation* **2020**, *16*, 236–244. [[CrossRef](#)]
33. Cui, D.; Ni, C. LncRNA Lnc712 Promotes Tumorigenesis in Hepatocellular Carcinoma by Targeting miR-142-3p/Bach-1 Axis. *Cancer Manag. Res.* **2020**, *12*, 11285–11294. [[CrossRef](#)] [[PubMed](#)]
34. Xie, M.; Sun, M.; Ji, X.; Li, D.; Chen, X.; Zhang, B.; Huang, W.; Zhang, T.; Wang, Y.; Tian, D.; et al. Overexpression of BACH1 mediated by IGF2 facilitates hepatocellular carcinoma growth and metastasis via IGF1R and PTK2. *Theranostics* **2022**, *12*, 1097–1116. [[CrossRef](#)] [[PubMed](#)]